NANO LETTERS

2004
Vol. 4, No. 11
2191−2196

Synthesis, Characterization, and Biological Application of Size-Controlled Nanocrystalline $NaYF_4$:Yb,Er Infrared-to-Visible Up-Conversion Phosphors

Guangshun Yi,*,†,‡ Huachang Lu,‡ Shuying Zhao,§ Yue Ge,§ Wenjun Yang,§ Depu Chen,*,‡ and Liang-Hong Guo*,§,||

Faculty of Materials Science & Engineering, Shandong University of Technology, Zibo 255049, China, Department of Chemistry, Tsinghua University, Beijing 100084, China, Beijing National Biochip Research & Engineering Center, 18 Life Science Parkway, Changping District, Beijing 102206, China, and Research Center for Eco-environmental Sciences, Chinese Acedemy of Sciences, 18 Shuangqing Road, Haidian District, Beijing 100085, China

Received August 15, 2004; Revised Manuscript Received September 21, 2004

ABSTRACT

Nanocrystalline infrared-to-visible up-conversion phosphors, ytterbium and erbium co-doped sodium yttrium fluoride, were synthesized. Spherical particles with narrow size distribution were prepared by a co-precipitation method in the presence of ethylenediaminetetraacetic acid (EDTA). Particles of controlled size in the range of 37 to 166 nm diameter were obtained by adjusting the molar ratio of EDTA to total lanthanides. Although the as-prepared nanoparticles emit very weak up-conversion fluorescence when excited by infrared light, the emission was enhanced by up to 40-fold after they were annealed at temperatures between 400 and 600 °C. By comparison with the bulk phosphor, the luminescence efficiency of the nanoparticle was estimated to be 1%. Factors affecting the particle size and their up-conversion fluorescence intensity were investigated by various microscopic and spectroscopic techniques. Preliminary results demonstrated the nanoparticles as promising up-converting fluorescence labels in the detection of biological interactions.

Phosphors are defined as solid, inorganic, crystalline materials that show luminescence upon excitation.[1] Those that emit lower energy photons when excited with higher energy photons are down-conversion phosphors. For example, ZnS:Mn and Y_2O_3:Eu, are well-known down-conversion phosphors.[2−5] On the other hand, phosphors that emit higher energy photons after absorbing lower energy excitation photons are up-conversion phosphors.[6] At least two lower energy photons are required to generate one higher energy photon. There is growing interest in studying up-conversion phosphors, because they are one of the most promising materials for the production of solid-state lasers, especially blue-light-emitting lasers. Up to now, red, green, and blue laser sources pumped by infrared light at room temperature have been reported.[7] Meanwhile, the use of up-conversion phosphors as fluorescent labels for the sensitive detection of biomolecules has attracted even more interest recently.[8−11]

Traditionally, most of the biological luminescent labels are organic dyes, such as rhodamine, fluorescein isothiocyanates (FITC), and cyanine dyes (Cy3, Cy5, and Cy7). More recently, metal and semiconductor nanocrystals have been employed as labels in biological detections.[12−13] The perceived advantages of the fluorescent nanocrystals are their high quantum yield, tuneable emission wavelength, and high stability against photobleaching. In comparison with down-conversion fluorescent materials, up-conversion fluorescent labels show very low background light due to their unique fluorescence properties. Excitation is performed using an infrared laser, which is compact, power-rich, and also inexpensive.[14] As with the down-conversion organic dyes, the up-conversion phosphors are usually stable, nonfading,

* Corresponding authors. Dr. G. Yi: Phone 86-10-62781691, Fax 86-10-62782485, E-mail yiguangshun@tsinghua.org.cn. Dr. D. Chen: Phone 86-10-62781691, Fax 86-10-62782485, E-mail chendp@chem.tsinghua.edu.cn. Dr. L.-H. Guo: Phone 86-10-62849339, Fax 86-10-62849339, E-mail LHGuo@mail.rcees.ac.cn.

† Shandong University of Technology.

‡ Tsinghua University.

§ Beijing National Biochip Research & Engineering Center.

|| Chinese Acedemy of Sciences.

10.1021/nl048680h CCC: $27.50
Published on Web 10/16/2004

and not significantly influenced by their environment (e.g., buffer pH or assay temperature, et al.).[15] By using 400 nm Y_2O_2S:Yb,Er up-conversion phosphors as labels, 1 ng/μL DNA was detected by Tanke's group, which is four times more sensitive than the test using Cy5 labels.[11] Y_2O_2S:Yb,Er up-conversion phosphors of 400 nm have also been found to be advantageous for use in the in vitro assay of biological compounds.[8,10,16] However, as a labeling material for biomolecules, especially for the sensitive determination of molecules such as DNA, RNA, or proteins, nanosized up-conversion phosphors with monodispersed size distribution and high luminescence efficiency are required.[11] The up-conversion phosphor reported in the above-mentioned literature is still too large.

Recently, Hirai[14] and Silver[17] described the preparation of nanocrystalline ytterbium and erbium co-doped yttrium oxide (Y_2O_3:Yb,Er) up-conversion phosphors. The mean size of the nanoparticles was 50 nm and 60 nm, respectively. In our previous paper,[18] nanocrystalline ytterbium and erbium co-doped lanthanum molybdate ($La_2(MoO_4)_3$:Yb,Er were synthesized via a hydrothermal method. The particle size of the nanoparticles was approximately 50 nm in diameter with a narrow size distribution. Reports in this area still remain scarce in the literature.

Ytterbium and erbium co-doped sodium yttrium fluoride (α-$NaYF_4$:Yb,Er) is among the most efficient infrared-to-visible up-conversion phosphors.[19−20] Its up-conversion efficiency is respectively 20 times and 6 times greater than that of La_2O_3:Yb,Er and $La_2(MoO_4)_3$:Yb,Er.[19] Although some chloride and bromide lattices show enhanced up-conversion luminescence intensity, most of them are sensitive to moisture.[21] They might not be suitable for labeling biomolecules, which are used mostly in aqueous solutions. Herein, we present a relatively simple and efficient route for the preparation of size-controlled $NaYF_4$:Yb,Er up-conversion nanoparticles with narrow size distribution. The synthesis begins with the rapid injection of a rare earth-EDTA complex into a vigorously stirred NaF solution to produce a homogeneous nucleation process. The average particle size is tuneable from 37 to 166 nm by varying the amount of EDTA. Factors affecting the particle size and their up-conversion fluorescence intensity were also studied. Transmission electron microscopy (TEM), X-ray diffraction (XRD), differential scanning calorimetry (DSC), X-ray fluorescence spectroscopy (XRF), inductively coupled plasma-mass spectrometry (ICP-MS), and photoluminescence spectroscopy (PL) are used to characterize the nanoparticles. To demonstrate their utility as up-converting fluorescence labels in biological detections, the $NaYF_4$:Yb,Er nanoparticles were coated with a layer of silica and then conjugated with goat anti-mouse antibody after surface silanization. Specific binding of the antibody-conjugated nanoparticles with an array of mouse IgG spotted on a chemically modified glass slide was detected on an up-conversion fluorescence image scanner.

Preparation of $NaYF_4$:Yb,Er nanoparticles is described in the Supporting Information section. The particles were first characterized by TEM shown in Figure 1. TEM allows the direct imaging of nanoparticles and provides information on the quality of individual particles, e.g., their size and size distribution. It can be seen from Figure 1a that the particles

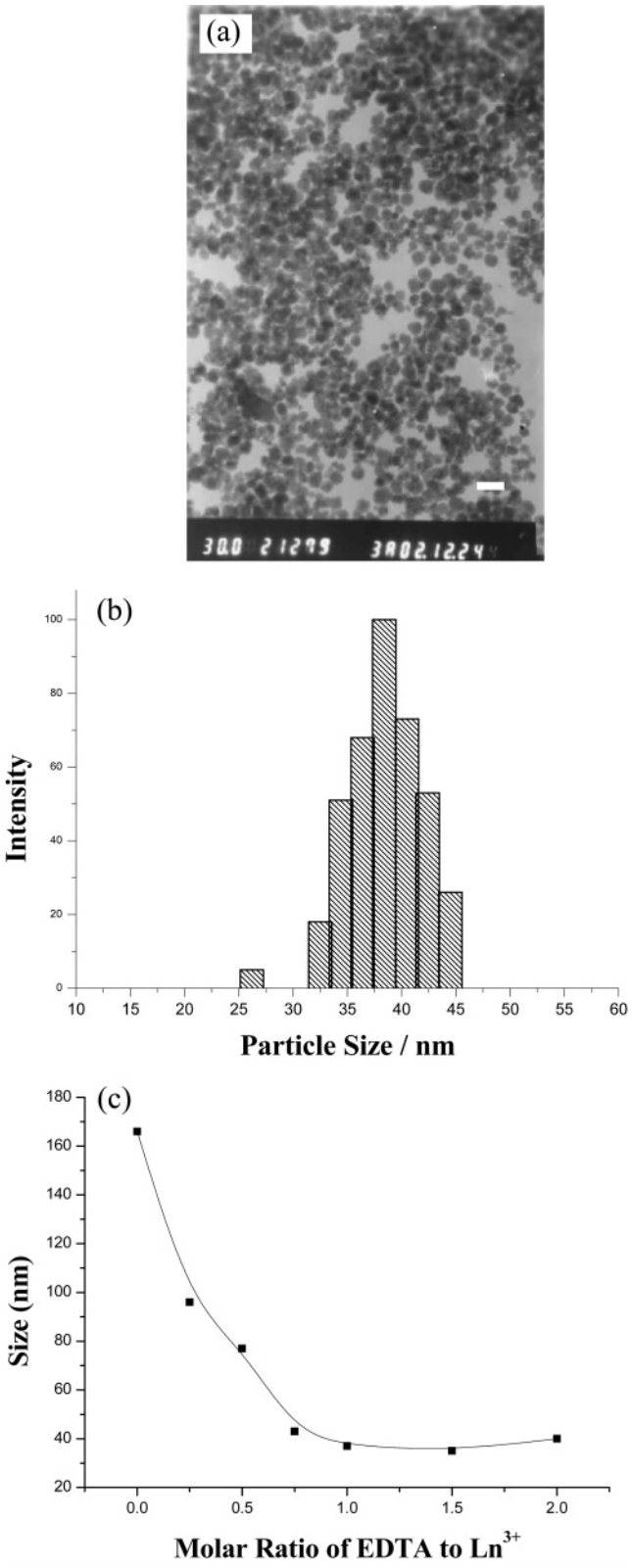

Figure 1. (a) TEM image of the as-prepared $NaYF_4$:Yb,Er nanoparticles obtained using a molar ratio of 1:1 EDTA/lanthanides. Bar = 100 nm. (b) Histogram of the size distribution of the $NaYF_4$:Yb,Er nanoparticles prepared in (a). (c) Relationship between TEM particle size and EDTA/Ln^{3+} ratio.

are spherical in shape with a mean diameter of approximately 40 nm. Also, the particles are reasonably uniform in size. The histogram of the particle diameter (Figure 1b) obtained from a particle size analyzer reveals that most of the particles are 32−46 nm in diameter, with an average value of about 38 nm. This result is in good agreement with the size estimated from the TEM image.

EDTA is an efficient chelator for rare earth ions. Its chelation constants (lgβ1) for Y^{3+}, Yb^{3+}, and Er^{3+} (collectively designated as Ln^{3+}) are 18.09, 19.51, and 18.85, respectively.[22] The presence of EDTA is found to be helpful for the formation of several types of ultrafine particles, such as Y_2O_3, PbS, CuS, and ZnS.[17,23−25] To investigate the effect of EDTA on the size of $NaYF_4$:Yb,Er particles in our synthetic method, the amount of EDTA was varied under the same precipitation condition to get a molar ratio of EDTA/Ln^{3+} of 0, 0.25, 0.5, 0.75, 1.0, 1.5, and 2.0. Typical TEM micrographs of the products are shown in the Supporting Information, from which it becomes obvious that the size of $NaYF_4$:Yb,Er is greatly influenced by the EDTA/Ln^{3+} ratio. A low EDTA/Ln^{3+} molar ratio resulted in large $NaYF_4$:Yb,Er nanoparticles, and vice versa. When the EDTA/Ln^{3+} ratio is above 1, the size of the $NaYF_4$:Yb,Er nanoparticles remains almost unchanged. The relationship between the particle size and EDTA/Ln^{3+} ratio is illustrated explicitly in Figure 1c.

As we know, EDTA is a strong chelator for rare earth ions; it reacts with Ln^{3+} to form stable Ln-EDTA (1:1) complexes. The roles of EDTA in the formation of size-controlled, monodispersed $NaYF_4$:Yb,Er nanoparticles can be postulated by applying the LaMer model.[26] According to the model, definite separation of nucleation and growth stages is the first requirement for uniform particle formation. As mentioned above, addition of chelating agents such as EDTA may have helped the separation between the two stages.[17,23−25] In addition, EDTA prevents particle coagulation by shielding the rare-earth metal ions, which is another necessity for the preparation of monodispersed particles. As for the size effect, chelation of the metal ions with EDTA should bring about decrease both in the nucleation process and in nuclei growth, but to a different extent, since the two processes lie in different concentration zones. In the presence of EDTA, the rare earth ions are presumably in a concentration zone more favorable to particle nucleation than growth, resulting in smaller particle size.

The composition of the 37 nm diameter nanoparticles was analyzed by sequential X-ray fluorescence spectrometry and ICP-MS. The analytical results indicate that the composition of the nanoparticles was $Na_{1.02}Y_{0.84}Yb_{0.13}Er_{0.03}F_{3.98}$ (Na 17%; Y 14.1%; Yb 2.1%; Er 0.4%; F 66.3%). There is some difference in the molar ratio of Y:Yb:Er between the particle product (0.84:0.13:0.03) and the solution reactants that were mixed to form the particle (0.80:0.17:0.03). This difference is a direct result of different chelating ability of EDTA with the three rare earth ions. As mentioned above, the chelation constants (lgβ1) for Y^{3+}, Yb^{3+}, and Er^{3+} are 18.09, 19.51, and 18.85, respectively. The stronger the metal ion chelates with EDTA, the less its content is in the final product.

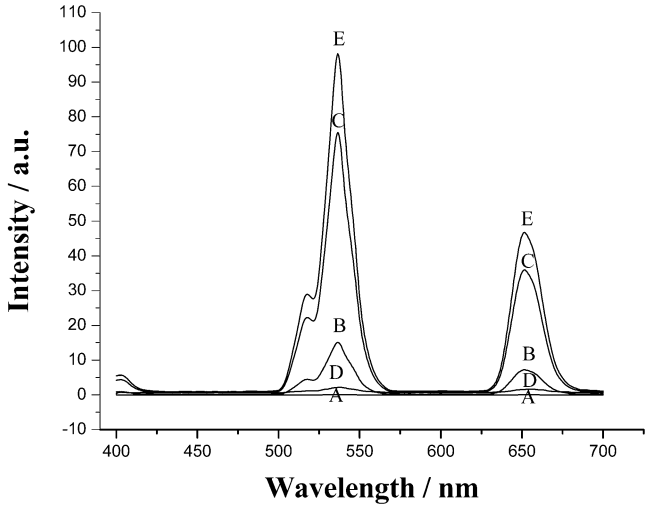

Figure 2. Up-conversion fluorescence spectra of the $NaYF_4$:Yb,Er nanoparticle solid synthesized with the addition of 1:1 EDTA/Ln^{3+}: (A) as-prepared; (B) annealed at 400 °C; (C) annealed at 600 °C; and (D) annealed at 700 °C. For comparison, the spectrum of the particles synthesized without addition of EDTA and annealed at 600 °C is also shown (E).

The $NaYF_4$:Yb,Er nanoparticles prepared in the co-precipitation procedure in the presence of EDTA had hardly any up-conversion fluorescence. However, after the nanoparticles were annealed at high temperatures for 5 h, bright up-conversion fluorescence was observed under the 980 nm infrared excitation. Figure 2 shows up-conversion fluorescence spectra of the $NaYF_4$:Yb,Er nanoparticle solid synthesized with 1:1 EDTA/Ln^{3+} and post-annealed for 5 h at different temperatures in the range of 400−700 °C. The fluorescent intensity increased remarkably with the increase of temperature from 400 °C to 600 °C, but decreased sharply and became very weak when the temperature reached 700 °C. The reason for the observed temperature effect will be discussed later.

There are three emission peaks at 517, 536, and 651 nm, which are assigned to the $^4H_{11/2}$ to $^4I_{15/2}$, $^4S_{3/2}$ to $^4I_{15/2}$, and $^4F_{9/2}$ to $^4I_{15/2}$ transitions of erbium, respectively.[27−29] Under 980 nm excitation, Er^{3+} absorbs one photon and its ground-state ($^4I_{15/2}$) electron is excited to the $^4I_{11/2}$ level. A second photon promotes the electron to the $^4F_{7/2}$ level. The excited electron decays first nonradiatively to $^2H_{11/2}$, $^4S_{3/2}$, and $^4F_{9/2}$ levels. When it decays further to the ground state, emission at 518, 537, and 652 nm occurs.

The spectrum of $NaYF_4$:Yb,Er nanoparticles described above was compared with that of the bulk phosphor prepared by a typical solid-state reaction. It can be seen from Figure 3 that the green fluorescence intensity of bulk phosphor is approximately four times stronger than that of the nanoparticles annealed at 400 °C. According to Page et al.,[30] the luminescence efficiency (defined as the emitted power divided by the power absorbed by the phosphor) of bulk $NaYF_4$:Yb,Er phosphor is 4%. Therefore, we can roughly estimate that the efficiency of the $NaYF_4$:Yb,Er nanoparticles is about 1%. The figure also reveals the difference in the up-conversion fluorescence spectrum between the bulk and nanoparticle materials. For the nanosized crystals, green

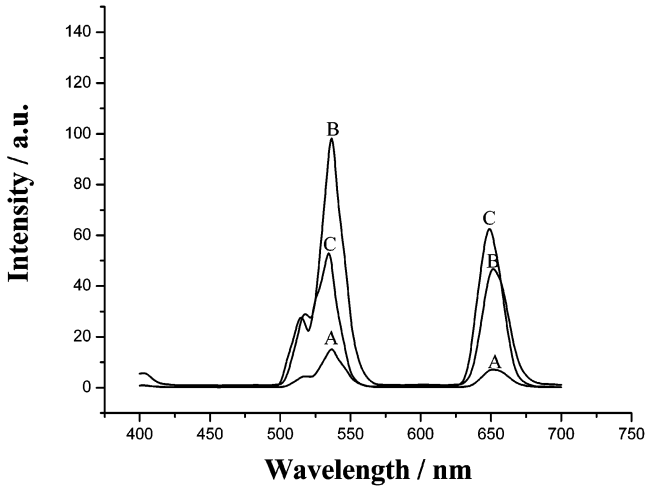

Figure 3. Up-conversion fluorescence spectra of $NaYF_4$:Yb,Er phosphors: (A) nanoparticles synthesized with EDTA/Ln^{3+} = 1 and annealed at 400 °C; (B) nanoparticles synthesized without addition of EDTA and annealed at 600 °C; and (C) bulk $NaYF_4$:Yb,Er phosphor prepared by a typical solid-state reaction.

emission at 517 and 536 nm is stronger than red (651 nm), while the opposite is true for the bulk phosphor. The reason for the difference is unclear to us at the moment.

Although the up-conversion fluorescence intensity of the nanoparticles annealed at 600 °C is the strongest, their size is not optimal if the particles are to be used as labels in biological detections. TEM images of the nanoparticles annealed at various temperatures reveals that, after annealing at 400 °C, the shape and size of the particles remained unchanged when compared with the as-prepared particles illustrated in Figure 1a. At higher temperatures, however, the particles started to aggregate into larger size and were no longer spherical in shape (see Supporting Information). For the best combination of particle size and fluorescence intensity, the optimal annealing temperature should be 400 °C.

To investigate the structural base for the effect of annealing temperature on the up-conversion fluorescence property of the $NaYF_4$:Yb,Er nanoparticles, XRD of the particles prepared with 1:1 EDTA/Ln^{3+} was performed. As shown in Figure 4, the particles annealed at different temperatures displayed distinctively different XRD patterns. A unique pattern was found for the as-prepared sample (Figure 4A), assigned to cubic phase $NaYF_4$:Yb,Er (ICDD, No. 77-2042). The crystallite size was calculated from the Scherrer's equation using the measured full width at half-maximum (fwhm) values of the XRD peaks. The fwhm value for the peak of maximum intensity (2θ = 28.153) B_1 is 0.232° (acquired from the X-ray diffractometer), B_0 = 0.104° (related to the instrument itself). The calculated crystallite size is 39.05 nm, which is in good agreement with that obtained from the TEM micrograph.

After annealing at 400 °C and 600 °C, a new, hexagonal $NaYF_4$:Yb,Er phase (ICDD No. 28-1192, also called α-NaYF4:Yb,Er) emerged in addition to the already existing cubic pattern, as shown in Figure 4B,C. This implies that the particles transformed partially from cubic phase to hexagonal phase by annealing. From 400 to 600 °C, the fraction of the hexagonal phase increased substantially, but the cubic phase was still present. When the temperature reached 700 °C, however, the hexagonal phase disappeared completely, and only the cubic phase remained (Figure 4D). It was also found that, for the samples prepared in the absence of EDTA, the cubic phase was transformed completely to the hexagonal phase at 600 °C, as shown in Figure 4E. This is different from the particles synthesized with addition of the chelator. The presence of EDTA seems to

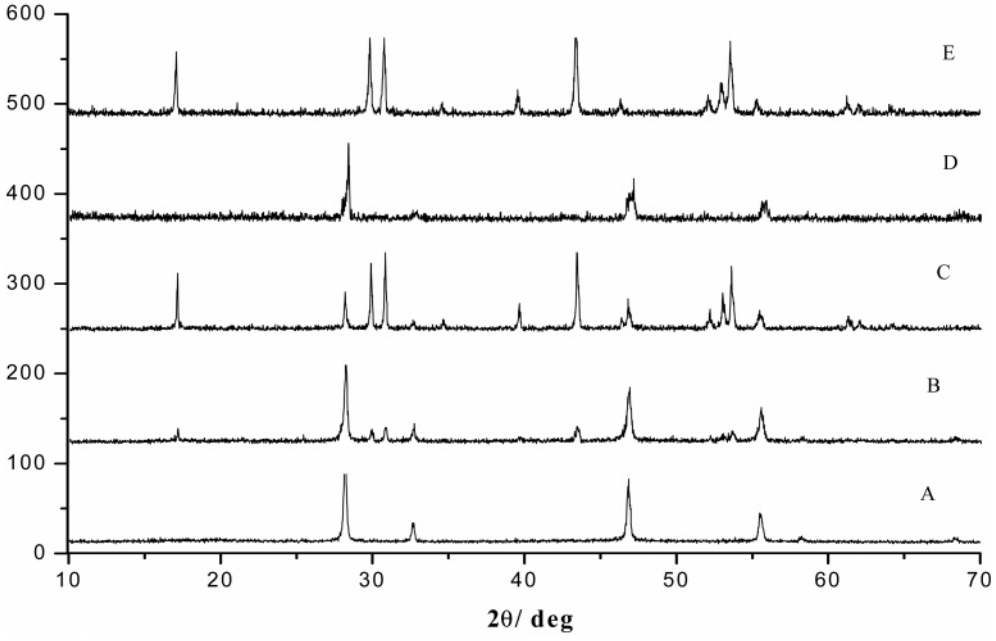

Figure 4. XRD patterns of the $NaYF_4$:Yb,Er nanoparticles synthesized with 1:1 EDTA/Ln^{3+}: (A) no annealing; (B) annealed at 400 °C; (C) annealed at 600 °C; (D) annealed at 700 °C; and (E) particles synthesized without EDTA and annealed at 600 °C.

suppress the phase transition. The phase transformation process was confirmed by the differential scanning calorimetry analysis. There was a sharp exothermic peak around 460 °C, which is within the temperature range investigated in the XRD experiment. The transformation from cubic to hexagonal phase is not unique to the $NaYF_4$:Yb,Er nanoparticles. In fact, it has been observed previously[31] with bulk $NaYF_4$ at temperatures above 600−700 °C. Putting together the fluorescence and XRD data, a connection seems to exist between the population of the hexagonal phase and the up-conversion fluorescence intensity of the nanosized $NaYF_4$:Yb,Er particles. Concurrent with the transformation of the particle from cubic to hexagonal phase after annealing at temperatures between 400 and 600 °C, the fluorescence intensity increased accordingly. As the hexagonal phase was transformed back to the cubic phase at 700 °C, the light intensity dropped as well. This observation, in combination with the fact that the hexagonal phase of the bulk $NaYF_4$:Yb,Er phosphor is most efficient in emitting up-conversion fluorescence,[32] suggests strongly that the hexagonal phase is also the major, if not the only component, which emits up-conversion fluorescence in the nanoparticles. However, as with the bulk material, it is still unclear why the hexagonal phase is more efficient than the cubic phase.

To demonstrate the utility of the up-conversion fluorescent nanoparticles as labeling material in biological detection, a preliminary experiment was carried out. The experiment employed mouse IgG/goat anti-mouse antibody as the model system. The antibody was conjugated to the nanoparticles and IgG was immobilized on a chemically modified glass slide. The nanoparticles annealed at 400 °C do not possess colloidal properties when dispersed in water. However, after the particles were coated with a shell of silica by the hydrolysis of tetraethyl orthosilicate, they became water soluble, with little decrease in their luminescence intensity. The silica shell was then silanized to introduce functional groups on the particle for antibody conjugation. Binding reaction between mouse IgG and antibody would result in the accumulation of surface-confined nanoparticles that could then be detected by up-conversion fluorescence. The experimental details are described in the Supporting Information. As shown in Figure 5, the first row of four positive control spots emit bright up-conversion fluorescence, indicating the image reader was functioning properly. The two rows of negative control spots did not show any signal, suggesting there was no nonspecific binding of the antibody−nanoparticle conjugate to the glass slide. Although there was no signal from the fourth row of 0.25 mg/mL IgG, higher concentration of IgG (1 mg/mL) spotted in the fifth row produced some weak but definitive image that looked similar to the positive control (Figure 5b). On a separate slide, the last row was spotted with an even higher concentration of IgG (3 mg/mL), and four bright spots were clearly seen in the image (Figure 5c). We therefore attribute the observed up-conversion fluorescence signal from the last row on the two slides to the binding of the antibody−nanoparticle conjugate specifically to the IgG molecules immobilized on the glass surface.

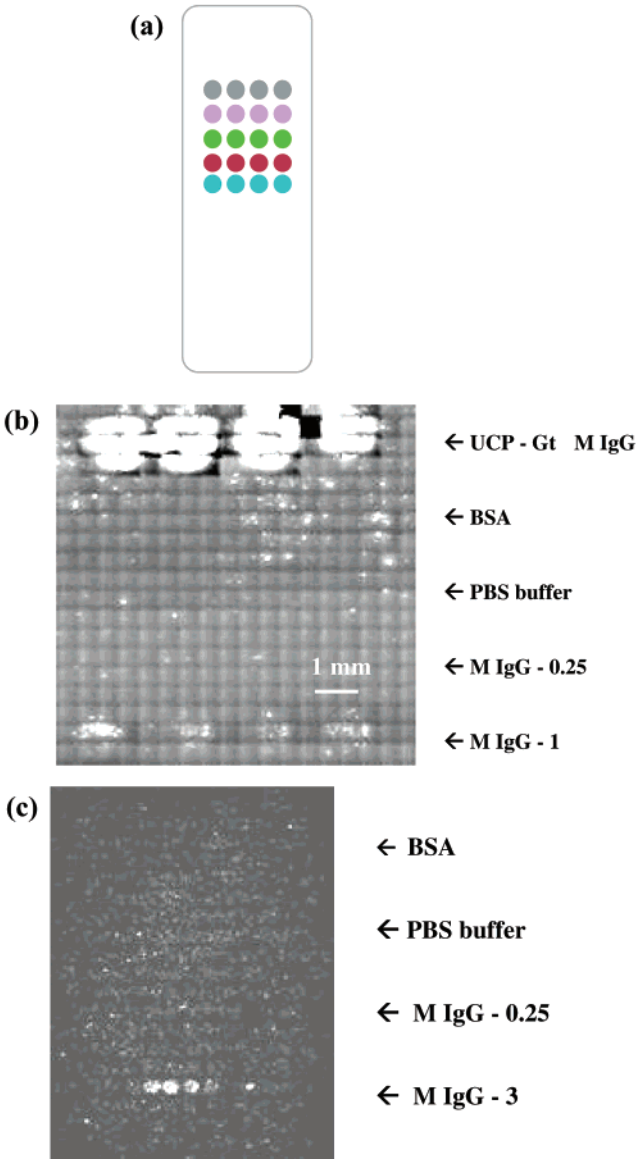

Figure 5. (a) Schematic of the 5×4 array spotted on an aldehyde-modified glass slide. First row: the nanoparticle−antibody conjugate as positive control. Second row: bovine serum albumin (BSA) as negative control. Third row: PBS buffer as negative control. Fourth row: 0.25 mg/mL mouse IgG. Fifth row: 1 mg/mL mouse IgG. (b) Up-conversion fluorescence image of the above array. (c) Image of a 4×4 array consisted of BSA, PBS, 0.25 mg/mL mouse IgG, and 3 mg/mL mouse IgG.

To conclude, $NaYF_4$:Yb,Er nanoparticles with narrow size distribution were prepared by co-precipitation of Y^{3+}, Yb^{3+}, Er^{3+} with NaF in the presence of EDTA. The particle size was controlled effectively in the range of 37 to 166 nm by adjusting the EDTA/Ln^{3+} ratio. After annealing at temperatures between 400 and 600 °C for 5 h, up-conversion fluorescence was observed with a luminescence efficiency of about 1%. Factors affecting the particle size and their up-conversion fluorescence intensity were investigated. The nanoparticles were characterized by TEM, XRD, DSC, XRF, and ICP-MS. Preliminary results demonstrated the nanoparticles as promising up-converting fluorescence labels in the detection of biological interactions.

Acknowledgment. Financial support from National Science Foundation of China (39989001, 39825108) and National Key Basic Research Development Program (G19990116) and a start-up fund from the Chinese Academy of Sciences is gratefully acknowledged.

Supporting Information Available: Experimental section and four additional figures of TEM images and fluorescence spectra of the nanoparticles. This material is available free of charge via the Internet at http://pubs.acs.org.

References

(1) Butler, K. H. *Fluorescent Lamp Phosphors*, Pennsylvania State University Press: University Park, 2003.
(2) Chen, W.; Sammynaiken, R.; Huang, Y. N. *J. Appl. Phys.* **2000**, *88*, 5188.
(3) Xie, P. B.; Zhang, W. P.; Yin, M.; Chen, H. T.; Zhang, W. W.; Lou, L. R.; Xia, S. D. *J. Colloid Interface Sci.* **2000**, *229*, 534.
(4) Konrad, A.; Fries, T.; Gahn, A.; Kummer, F.; Herr, U.; Tidecks, R.; Samwer, K. *J. Appl. Phys.* **1999**, *86*, 3129.
(5) Sharma, P. K.; Nass, R.; Schmidt, H. *Opt. Mater.* **1998**, *10*, 161.
(6) Tropper, A. C.; Carter, J. N.; Lauder, R. D. T.; Hanna, D. C.; Davey, S. T.; Szebesta, D. *J. Opt. Soc. Am.* **1994**, *11*, 886.
(7) Sandrock, T.; Scheife, H.; Heumann, E.; Huber, G. *Opt. Lett.* **1997**, *22*, 808.
(8) Corstjens, P.; Zuiderwijk, M.; Brink, A.; Li, S.; Feindt, H.; Neidbala, R. S.; Tanke, H. *Clin. Chem.* **2001**, *47*, 1885.
(9) Corstjens, P. L. A. M.; Zuiderwijk, M.; Nilsson, M.; Feindt, H.; Niedbala, R. S.; Tanke, H. J. *Anal. Biochem.* **2003**, *312*, 191.
(10) Hampl, J.; Hall, M.; Mufti, N. A.; Yao, Y. M. M.; MacQueen, D. B.; Wright, W. H.; Cooper, D. E. *Anal. Biochem.* **2001**, *288*, 176.
(11) van de Rijke, F.; Zijlmans, H.; Li, S.; Vail, T.; Raap, A. K.; Niedbala, R. S.; Tanke, H. J. *Nat. Biotechnol.* **2001**, *19*, 273.
(12) Niemeyer, C. M. *Angew. Chem., Int. Ed.* **2001**, *40*, 4128.
(13) Parak, W. J.; Gerion, D.; Pellegrino, T.; Zanchet, D.; Micheel, C.; Williams, S. C.; Boudreau, R.; Le Gros, M. A., Larabell, C. A.; Alivisatos, A. P. *Nanotechnology*, **2003**, *14*, R15.
(14) Hirai, T.; Orikoshi, T.; Komasawa, I. *Chem. Mater.* **2002**, *14*, 3576.
(15) Beverloo, H. B.; van Schadewijk, A.; Zijlmans, H. J. M. A. A.; Tanke, H. J. *Anal. Biochem.* **1992**, *203*, 326.
(16) Zijlmans, H. J. M. A.; Bonnet, J.; Burton, J.; Kardos, K.; Vail, T.; Niedbala, R. S.; Tanke, H. J. *Anal. Biochem.* **1999**, *267*, 30.
(17) Silver, J.; Martinez-Rubio, M. I.; Ireland, T. G.; Fern, G. R.; Withnall, R. *J. Phys. Chem. B* **2001**, *105*, 948.
(18) Yi, G. S.; Sun, B. Q.; Yang, F. Z.; Chen, D. P.; Zhou, Y. X.; Cheng, J. *Chem. Mater.* **2002**, *14*, 2910.
(19) Blasse, G.; Grabmaier, B. C. *Luminescent Materials*; Springer: Berlin, 1994.
(20) Hehlen, M. P.; Philips, M. L. F.; Cockroft, N. J.; Gudel, H. U. In *Encyclopedia of Materials: Science and Technology*; Burschow, K. H. J. Ed.; Elsevier Science Ltd.: New York, 2001.
(21) Egger, P.; Rogin, P.; Riedener T. *Adv. Mater.* **1996**, *8*, 688.
(22) Huang, C. *Coordination Chemistry of Rare Earth Elements*; Science Publishing Press: Beijing, 1997.
(23) Chiu, G. *J. Colloid Interface Sci.* **1974**, *49*, 160.
(24) Chiu, G. *J. Colloid Interface Sci.* **1977**, *1977*, 193.
(25) Chiu, G. *J. Colloid Interface Sci.* **1981**, *83*, 309.
(26) Sugimoto T. *Adv. Colloid Interface Sci.* **1987**, *28*, 65.
(27) Chamarro, M. A.; Cases, R. *J. Lumin.* **1990**, *46*, 59.
(28) Zhao, S. L.; Hou, Y. B.; Sun, L. *J. Northern Jiaotong University* **2000**, *24*, 89.
(29) Shojiya, M.; Takahashi, M.; Kanno, R.; Kawamoto, Y.; Kadono, K. *Appl. Phys. Lett.* **1994**, *65*, 1874.
(30) Page, R. H.; Schaffers, K. I.; Waide, P. A.; Tassano, J. B.; Payne, S. A.; Krupke W. F. *J. Opt. Soc. Am. B* **1998**, *15*, 996.
(31) Thomas, R. E.; Insley, H.; Hebert, G. M. *Inorg. Chem.* **1966**, *5*, 1222.
(32) Kramer, K. W.; Biner, D.; Frei, G.; Gudel, H. U.; Hehlen, M. P.; Luthi, S. R. *Chem. Mater.* **2004**. DOI 10.1021/cm031124o.

NL048680H